A neural mass model with neuromodulation

Damien Depannemaecker, Chloe Duprat, Marianna Angiolelli, Carola Sales Carbonell, Huifang Wang, Spase Petkoski, Pierpaolo Sorrentino, Hiba Sheheitli, Viktor Jirsa

A neural mass model with neuromodulation

Damien Depannemaecker[1✉], Chloe Duprat[1], Marianna Angiolelli[1,2], Carola Sales Carbonell[1], Huifang Wang[1], Spase Petkoski[1], Pierpaolo Sorrentino[1], Hiba Sheheitli*[1,3,4], Viktor Jirsa*[✉1]

[1]Aix Marseille Univ, INSERM, INS, Inst Neurosci Syst, Marseille, France
[2]Department of Engineering, Università Campus Bio-Medico di Roma, Rome, Italy
[3]Department of Neurology, University of Minnesota, Minneapolis, MN, United States
[4]Department of Psychiatry and Behavioral Sciences, University of Minnesota, Minneapolis, MN, United States

✉ damien.depannemaecker@univ-amu.fr, viktor.jirsa@univ-amu.fr

*co-last authors

Abstract

The study of brain activity and its function requires the development of computational models alongside experimental investigations to explore different effects of multiple mechanisms at play in the central nervous system. Chemical neuromodulators such as dopamine play central roles in regulating the dynamics of neuronal populations. In this work, we propose a modular framework to capture the effects of neuromodulators at the neural mass level. Using this framework, we formulate a specific model for dopamine dynamics affecting D1-type receptors. We detail the dynamical repertoire associated with dopamine concentration evolution. Finally, we give one example of use in a basal-ganglia network in healthy and pathological conditions.

1 Introduction

Neuromodulators, such as dopamine and serotonin, play central roles in regulating the dynamics of neuronal populations within the central nervous system. These biochemical agents modulate the activities of multiple neurons simultaneously, acting on the global dynamics of the brain.

At the synaptic level, neuromodulators can modify the strength of connections between neurons, impacting synaptic transmission and plasticity. Additionally, they can regulate the intrinsic excitability of neurons, influencing their firing rates and patterns of activity [38, 42].

On a broader scale, neuromodulators contribute to the synchronization and coordination of neuronal ensembles, thereby shaping network dynamics involved in various cognitive and behavioral processes [4,15,40,45,49,51]. For instance, dopamine is implicated in reward processing, motivation and motor control [5], while serotonin is associated with mood regulation, sleep-wake cycles, and emotional processing. Serotonin dysregulation has been associated with mood disorders such as depression and anxiety disorders [27, 36].

Understanding the intricate interplay between neuromodulators and brain function as expressed in the electrophysiological activity of the neuronal populations is fundamental for elucidating the neural mechanisms underlying complex brain functions and disorders.

Dopaminergic pathways are related to cognitive processes and behaviors such as wakefulness, working memory, and cognitive control [44]. Aging-related changes in dopaminergic regulation have been linked to cognitive performance [3], and they were hypothesized to play a crucial role in the dynamic compensation as a marker of improved cognitive abilities during aging [26]. By incorporating the effects of various neuromodulators, we can better understand the differences in cognitive decline associated with aging [7].

At the same time, neuromodulation impairment, in particular of dopamine, has been linked to the occurrence of different neurological disorders [24], such as Parkinson's disease (PD) or Schizophrenia [23].

The pathophysiology of PD is characterized by the degeneration of dopamine-producing neurons in the substantia nigra of the basal ganglia, leading to the loss of dopaminergic nigrostriatal neurons along the nigrostriatal pathways, with milder losses in the mesolimbic and mesocortical circuits. To model the neuromodulatory aspects of these pathways within personalized whole-brain networks we need to focus on structural changes, particularly within the basal ganglia-thalamocortical circuit [2].

PD and psychiatric disorders represent distinct categories of neurological conditions, each characterized by its clinical features and prevalence. PD, as the second most prevalent neurodegenerative disorder, primarily manifests motor symptoms, including tremors, rigidity, and bradykinesia, alongside a range of non-motor symptoms. The prevalence of PD varies with age, affecting 0.04% of individuals in the 40-49 age group and rising to 2% in those aged over 80 [2, 39]. On the other hand, psychiatric disorders encompass a heterogeneous group of conditions resulting in disruptions to cognitive processes, emotional regulation, and behavior. These disorders affected a staggering

970 million individuals worldwide in 2019, as reported by the World Health Organization [37]. Psychiatric disorders regroup a broad diversity of diseases but to exemplify, Schizophrenia affects approximately 24 million individuals globally.

Psychiatric disorders entail distinctive neuromodulatory mechanisms. Here, the pathophysiology revolves around dysfunctions in neurotransmission and neuromodulation, primarily featuring the mesolimbic dopamine pathway. This pathway, extending from the ventral tegmental area to limbic regions, takes a central role in the generation of positive psychotic symptoms integral to Schizophrenia. To integrate neuromodulatory pathways into whole-brain network models, we need to take into account the inter-regional connection between source and target regions in conjunction with other region-specific parameters enhancing our comprehension of the intricate interplay of mechanisms contributing to the emergence of psychiatric disorders [31, 34].

Furthermore, both PD and psychiatric disorders exhibit broader-scale dynamic phenomena. In the context of PD, aberrant dynamics within the basal ganglia result in anomalous bursts of activity in the beta frequency range, a phenomenon closely associated with clinical disability [52]. Similarly, in psychiatric disorders, there is a disruption in the balance between excitation and inhibition within cortical regions. This imbalance may result from synaptic pruning or alterations in neurotransmitter systems, contributing to the pathophysiology of these conditions [16, 20].

Deep brain stimulation emerges as an intervention strategy aimed at "desynchronizing" neural activity in both conditions, with computational modeling studies playing a pivotal role in exploring the underlying mechanisms. These models enable the prediction of optimal stimulation patterns in silico, thereby informing treatment design and deepening our understanding of these disorders [14, 29, 48, 53].

Additionally, the application of brain network models extends to the classification and differentiation of various forms of these neurological conditions. Recent studies underscore the potential of enhancing the classification of PD patients or individuals with psychiatric disorders by supplementing empirical data with simulated data generated from patient-specific brain network models [22].

Integrating personalized whole-brain network models and computational methodologies [50] should contribute to our understanding of the dynamic aspects of these disorders, facilitating refined treatment strategies and a deeper comprehension of their multifaceted etiologies, as it has been done previously for other conditions, such as epilepsy [9].

The aim is to create a model that reflects how neuromodulators influence the electrophysiological activity patterns in the human brain, to be implemented into the simulated environment of The Virtual Brain (TVB) [43]. The desired model should provide a level of detail closely resembling real

human data, specifically focusing on the mesoscopic scale to align with TVB's scope for simulating neural dynamics [1]. It is crucial to consider the impact of degeneracy and multi-realizability [13] (i.e. multiple models or parmetrizations leads to similar observable behaviors), as well as experimental challenges associated with biophysical mechanisms that are difficult to access, which could impede the interpretability of the model.

The selected model should incorporate identifiable and measurable biophysical mechanisms, ensuring a comprehensive understanding of neural dynamics. Additionally, it should allow for a diverse range of dynamic behaviors and account for various inhibitory and excitatory connections to capture how neuromodulation affects different receptors.

To tackle this challenge, this paper introduces a generic framework for modeling neuromodulator dynamics within a neural mass model. We specifically concentrate on dopamine by presenting a tailored formulation of the model. This includes an examination of how dopamine dynamics influence neural activity and concludes with a brief example application involving a model of the basal ganglia network.

2 Methods

The chosen model is a neural-mass model [6], utilizing a mean-field approach [35]. This model is derived from the adaptive quadratic integrate-and-fire model (aQIF) of individual neurons [18]. It enables the consideration of different conductance-based synaptic inputs.

Next, we aim to include neuromodulation as a variable in our model. We follow the formalism adopted by Kringelbach et al. [25], which introduces the effects of serotonin on the neural mass level as an additive current using the Michaelis-Menten equation [21,32]. In their work, the impact of serotonin was introduced as an additive current denoted as M within the excitability model.

In our study, we adapt this formalism to account for the generic dynamics of neuromodulators. We propose using the Michaelis-Menten equation to model the evolution of neuromodulator concentration and introducing its modulatory effect, denoted as M, as a modulation of the synaptic conductances rather than as an additive current. This modification aims to enhance the precision and relevance of our model in capturing the nuanced influence of neuromodulators on neural excitability. Then we propose a specific application to dopamine, with a possible further reduction for this specific case brought about by the relatively slow timescale of dopamine concentration evolution. In the following subsection, we detail the model construction.

2.1 Neural mass model

The equations of the neural dynamics are modified from the work of Chen and Campbell [6] and Sheheitli [46], to obtain a neural mass model capturing the dynamics of a population of N neurons. Following the Lorentzian ansatz [35], which assumes in the thermodynamic limit $N \to \infty$, the distribution of the membrane voltage will converge to Lorentzian-shaped function, regardless of the initial conditions, additive currents η_i are assumed to be distributed according to a Lorentzian distribution with a half-width Δ, and centered at $\bar{\eta}$. The variables correspond to the firing rate r, the mean membrane potential V and the adaptation u. We consider conductance-based synapses, excitatory with AMPA receptors of maximal conductance g_a and reversal potential E_a, and inhibitory with GABA receptors of maximal conductance g_g and reversal potential E_g. The resulting mean-field equations hence become:

$$\frac{dr}{dt} = 2arV + br - g_a r S_a - g_g S_g + \frac{a\Delta}{\pi} \tag{1}$$

$$\frac{dV}{dt} = aV^2 + bV + c + \eta - \frac{\pi^2 r^2}{a} + g_a S_a (E_a - V) + g_g S_g (E_g - V) + I_{\text{ext}} - u \tag{2}$$

$$\frac{du}{dt} = \alpha(\beta V - u) + u_d r \tag{3}$$

$$\frac{dSa}{dt} = -\frac{S_a}{\tau_{\text{Sa}}} + S_{j_a} c_{\text{exc}} + J_a r \tag{4}$$

$$\frac{dSg}{dt} = -\frac{S_g}{\tau_{\text{Sg}}} + S_{j_g} c_{\text{inh}} \tag{5}$$

$$\tag{6}$$

We use this set of equations as a neural mass model, i.e. low-dimensional representation that captures the excitability dynamics of a neuronal population. On this basis, we introduce the dynamics of neuromodulation, and in particular of dopamine.

2.2 Generic equations for neuromodulation

Two aspects are important in neuromodulation dynamics. First, the availability of the neuromodulator is considered, i.e. the evolution of the local concentration. Secondly, its effect on neural activities through specific receptors. One equation for each type of chemical neuromodulation (i.e. capturing the evolution of the concentration) and one equation for each receptor type (i.e. capturing the activation of each of these receptors) are necessary. The functional form for the concentration is made of two terms, where the first one corresponds to the mechanisms leading to

the increase of the local concentration. Most neuromodulators depend on the activity of a specific brain region that is afferent to the considered node. The second term corresponds to its decrease, due to re-uptake mechanisms that can be captured by Michaelis-Manten formalism. In the following subsection, we describe the construction of the equation specific for dopamine. The variable denoted M, captures the proportion of specific receptors activated by the neuromodulator. The typical functional form is a sigmoid function, the parametrization that must be specific for each receptor type. If the receptor has an enhancing effect, the slope is positive; and conversely for diminishing effect. Then the M variable enters the mean membrane potential equation according to the considered receptor's specific biophysical properties. It can either modulate a non-synaptic conductance through an additional term of the form $Mg_i(E_i - V)$ with g_i and E_i associated with a charged molecule or directly modulate the synaptic conductances, as it is the case for dopamine. In the following subsection, we take the example of D1 receptors modulating the conductance of AMPA synapses.

2.2.1 Dopamine reuptake

The reuptake of dopamine is a process in which dopamine is returned to the presynaptic neuron from the synaptic cleft. The primary molecular mechanism responsible for dopamine reuptake involves a protein known as the dopamine transporter (DAT). The reuptake process can be described by the following simplified equation:

$$[D_p]_e + \text{DAT} \xrightarrow{\text{Reuptake}} [D_p]_i$$

In this equation: $[D_p]_e$ represents dopamine molecules in the extracellular space, DAT represents the dopamine transporter protein on the neuron membrane, and $[D_p]_i$ represents dopamine molecules that have been taken back into the neuron.

The dopamine transporter (DAT) actively transports dopamine from the extracellular space back into the presynaptic neuron, terminating the signal transmission at the synapse. This reuptake process is crucial for regulating the dopamine concentration in the synaptic cleft and maintaining proper neurotransmission. Additionally, it serves as a target for various drugs, including certain antidepressants and psychostimulants, which can modulate dopamine reuptake.

2.2.2 Michaelis-Menten Formalism for Dopamine Reuptake

The dynamics of dopamine reuptake can be described using Michaelis-Menten (M-M) formalism, which involves applying the M-M equation to represent the process of dopamine transport via the dopamine transporter (DAT).

The general form of the M-M equation is:

$$V = \frac{V_{\max} \cdot [S]}{K_m + [S]}$$

and is a mathematical description of the relationship between substrate concentration $[S]$ and reaction rate V, characterized by the maximum reaction rate (V_{max}) and the Michaelis constant (K_m). We can adapt this equation to describe the dynamics of dopamine reuptake:

$$V_{Dpr} = \frac{V_{\max} \cdot [D_p]_e}{K_m + [D_p]_e}$$

where: V_{Dpr} is the reuptake rate and represents the velocity dopamine returns to the neuron. $V_{\max}$ is the maximum reuptake rate, which corresponds to the rate when the dopamine transporter (DAT) is fully saturated with dopamine. K_m is the Michaelis constant, representing the extracellular dopamine concentration at which the reuptake rate is half of $V_{\max}$. $[D_p]_e$ is the concentration of dopamine in the extracellular space.

This formulation is a simplification, and the actual dynamics of dopamine reuptake are influenced by various factors, including the number and activity of dopamine transporters, the membrane potential, and the presence of other substances that may modulate reuptake.

It's important to note that while the M-M formalism provides a useful approximation for enzymatic-like processes, but may not capture all the complexities involved in dopamine dynamics within the synapse. More sophisticated models may be necessary to achieve a more detailed mechanistic understanding of neurotransmitter reuptake kinetics. In our case, we are interested in the global phenomenon leading to the regulation of the electrophysiological activities of a whole population of neurons.

The local concentration will increase thanks to the projection from dopaminergic neurons, through the dopaminergic coupling c_{dopa}, scaled in each efferent region by a factor k:

$$V_{Dpi} = kc_{dopa}$$

Thus, the change over time (with time constant τ_{Dp}) in the extracellular dopamine concentra-

tion corresponds to the difference between the rate of local input and the rate of reuptake:

$$\tau_{Dp}\frac{d[D_p]_e}{dt} = V_{Dpi} - V_{Dpr} \tag{7}$$

Given the M-M equation for dynamics of dopamine reuptake and the local dopamine concentration, we obtain:

$$\tau_{Dp}\frac{d[D_p]_e}{dt} = kc_{\text{dopa}} - \frac{V_{\max}[D_p]_e}{K_{\text{m}} + [D_p]_e} \tag{8}$$

Considering that variations in dopamine concentration occur much more slowly than the firing rate dynamics and, therefore, it does not impact the derivation of the mean-field associated with fast variables.

2.2.3 Modulatory dynamics for D1 receptors

The given equation represents a mathematical model describing the dynamics of receptors within the populations. It uses a phenomenological activation function and an exponential decrease over time. It can be specifically formulated for the D1-type dopamine receptor.

$$\tau_m\frac{dM_{D1}}{dt} = -M_{D1} + \frac{R_d}{1+\exp(-S_p([D_p]_e+1))}$$

Where: M_{D1} is the modulation effect associated with the D1-type dopamine receptor. The modulation effect decreases over time ($-M_{D1}$). R_d is the receptor density in a given receptor population. $[D_p]_e$ is the extracellular dopamine concentration. S_p is a parameter that influences the sensitivity of the receptor to changes in extracellular dopamine concentration. The term $\frac{R_d}{1+\exp(S_p([D_p]_e+1))}$ represents the influence of extracellular dopamine on the modulation effect. The sigmoidal function introduces a non-linear activation of the receptor and simulates a saturation effect as dopamine concentration increases.

2.3 Neural mass model including neuromodulation

The modeling framework proposed here aims to enable formulation for different neuromodulator and receptor types (see Figure 1). Since our primary focus is on the impact of dopamine dynamics within the basal ganglia, as discussed in the next section, we focus on this specific neuromodulator and its corresponding receptors. This scenario serves as our example for specifying the model. The dopamine affects the AMPA excitatory conductances [47]. In that case, the M_D variable modulates

the conductance g_a through the term $M_D + B$, the variable M_D evolves in a range from 0 to R_d and $B = 1$ is the basal level to enable the minimal AMPA conductance even in the absence of modulation by the extracellular dopamine $[D_p]$.

$$\frac{dr}{dt} = 2arV + br - g_a S_a r - g_g S_g + \frac{a\Delta}{\pi} \tag{9}$$

$$\frac{dV}{dt} = aV^2 + bV + c + \eta - \frac{\pi^2 r^2}{a} + (M_D + B) g_a S_a (E_a - V) + g_g S_g (E_g - V) - u + I_{ext} \tag{10}$$

$$\frac{du}{dt} = \alpha(\beta V - u) + u_d r \tag{11}$$

$$\frac{dS_a}{dt} = \frac{-S_a}{\tau_{S_a}} + S_{ja} c_{exc} + J_a r \tag{12}$$

$$\frac{dS_g}{dt} = \frac{-S_g}{\tau_{S_g}} + S_{jg} c_{inh} \tag{13}$$

$$\tau_{Dp} \frac{d[D_p]}{dt} = k c_{dopa} - \frac{V_{max}[D_p]}{(K_m + [D_p])} \tag{14}$$

$$\tau_m \frac{dM_{D1}}{dt} = -M_{D1} + \frac{R_d}{1 + exp(-S_p([D_p]_e + 1))} \tag{15}$$

With this formalism, other neuromodulators can be introduced, with an additional variable of the same form as equation 14 for each of them. Then multiple types of receptors can be considered [33], and each of the receptor dynamics would take the same form as the equation 15. Finally, the modulatory equation of each type of receptor would enter the equation 10 of the mean membrane potential according to its biophysical properties and either affect one of the synaptic conductance and/or an additional conductance. The framework is schematized in Figure 1.

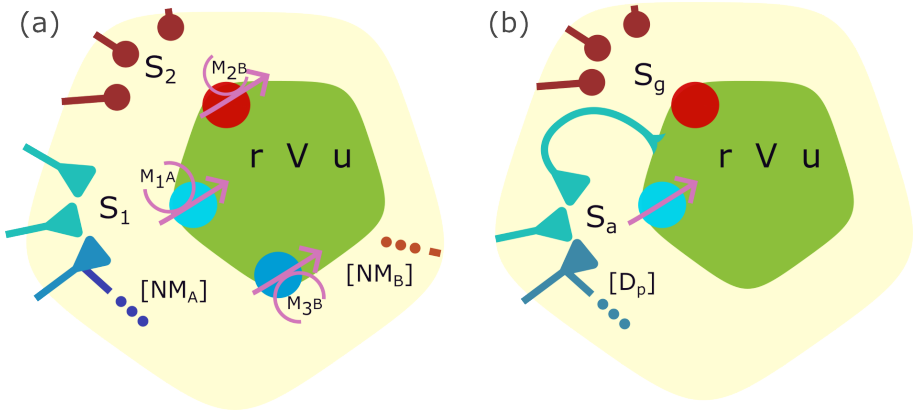

Figure 1: Schematic of the model. (a) A generic neural mass model framework with neuromodulation. Neural activity is characterized by the firing rate r, the mean membrane potential V, and mean adaptation u. It receives different synaptic inputs $S_1, S_2, \ldots$, and undergoes modulation through receptors $M_1, M_2, M_3, \ldots$ associated with different neuromodulators $NM_A, NM_B, \ldots$ released by projecting neurons. The modulation can affect either post-synaptic receptors (e.g., M_1 or M_2 in the schematic) or receptors on the neuronal membrane (e.g., M_3). This flexible framework allows for the consideration of multiple neuromodulators and receptors as needed by the scientific question. (b) The model schematic for a neural mass model, as introduced in section 2.3. It can be parameterized for excitatory AMPA and inhibitory GABA synapses, with activation variables S_a and S_g, respectively. It also accounts for self-recurring connections to excitatory inputs. Moreover, it can be tailored for specific cases such as dopamine ($[D_p]$) modulation, which linearly affects AMPA conductance.

M can be removed by adiabatic reduction. Indeed the modulation occurs in the same order of time scale as the concentration evolution and is thus strongly correlated with $[D_p]$ variables. By considering the linear part of the sigmoid of the M_{D1} equation (specific for D1 receptors), we obtain the linear relation with the form $A_{D1}[D_p] + B_{D1}$, then the equations become:

$$\frac{dr}{dt} = 2arV + br - g_a S_a r - g_g S_g r + \frac{a\Delta}{\pi} \tag{16}$$

$$\frac{dV}{dt} = aV^2 + bV + c + \eta - \frac{\pi^2 r^2}{a} + (A_{Dp}[D_p] + B_{Dp}) g_a S_a (E_a - V) + g_g S_g (E_g - V) - u + I_{ext} \tag{17}$$

$$\frac{du}{dt} = \alpha(\beta V - u) + u_d r \tag{18}$$

$$\frac{dS_a}{dt} = \frac{-S_a}{\tau_{S_a}} + S_{ja} c_{exc} + J_a r \tag{19}$$

$$\frac{dS_g}{dt} = \frac{-S_g}{\tau_{S_g}} + S_{jg} c_{inh} \tag{20}$$

$$\frac{d[D_p]}{dt} = k c_{dopa} - \frac{V_{max}[D_p]}{(K_m + [D_p])} \tag{21}$$

3 Results

We studied the emerging dynamics of this model. We started with a bifurcation analysis of the fast sub-system constituted by the $r - V$ variables. Through numerical simulations, we characterized the model's behaviors for different connectivity weights and dopamine inputs. Finally, we built a small network corresponding to the basal ganglia and showed how changes in neuromodulation dynamics lead to the emergence of dynamics in the frequency band comparable to those described in pathological conditions such as PD [30].

3.1 V-r dynamics

The system of equations obtained enables a rich dynamical repertoire. To analyze it, we first isolated the fast variables r and V associated with the activity of the firing rate and mean membrane potential. Other variables are fixed and serve as bifurcation parameters to study their effects on the fast dynamics, as commonly done in slow-fast system analysis [10, 19, 41].

We consider the case of an excitatory neural mass, the parameters (adapted from [6]) are given in table 5. We set S_g to 0 (as it refers to inhibitory GABAergic inputs, not considered here) and studied the effects of the variation of adaptation u, AMPA excitatory synaptic activation S_a, and dopamine concentration $[D_p]$ on the structure of the dynamics of the $r - V$ sub-system.

With different sets of parameters, we observe a vast diversity of qualitative behaviors in Figure 2. One is associated with a low firing rate and mean membrane potential around the resting state for mean membrane potential. Two fixed points coexist, a r-positive stable node, and, a r-negative unstable node (Figure 2a). Oscillatory behaviors corresponding to a limit cycle in the $r - V$ sub-system can be found (Figure 2b). We can obtain similar oscillatory behaviors with completely different settings of fixed variables of the slow sub-system. $[D_p]$ and S_a values are based on $c_{exc} = 0.017$ and $c_{dopa} = 1e-5$ (which are in the range of values for the full-network analysis) (Figure 2c). Dump oscillations are observed, within the configuration presented here, the co-existence of stable focus and unstable focus (Figure 2d). We also observe more complex regimes where four fixed points exist. In the first situation, we observe three r-positive fixed points and one r-positive fixed point of which only one stable fixed node with a low firing rate and mean membrane potential close to resting state value (Figure 2e). In the second situation, we observe one r-positive fixed point and three r-positive fixed points of which only 1 stable fixed focus with a higher firing rate and mean membrane potential close to resting state value (Figure 2f). Due to the presence of stable

attractors for realistic negative firing rates in certain configurations, we should ensure that during the use of this model for the simulation of brain activities, the trajectory stays into r-positive basins of attraction.

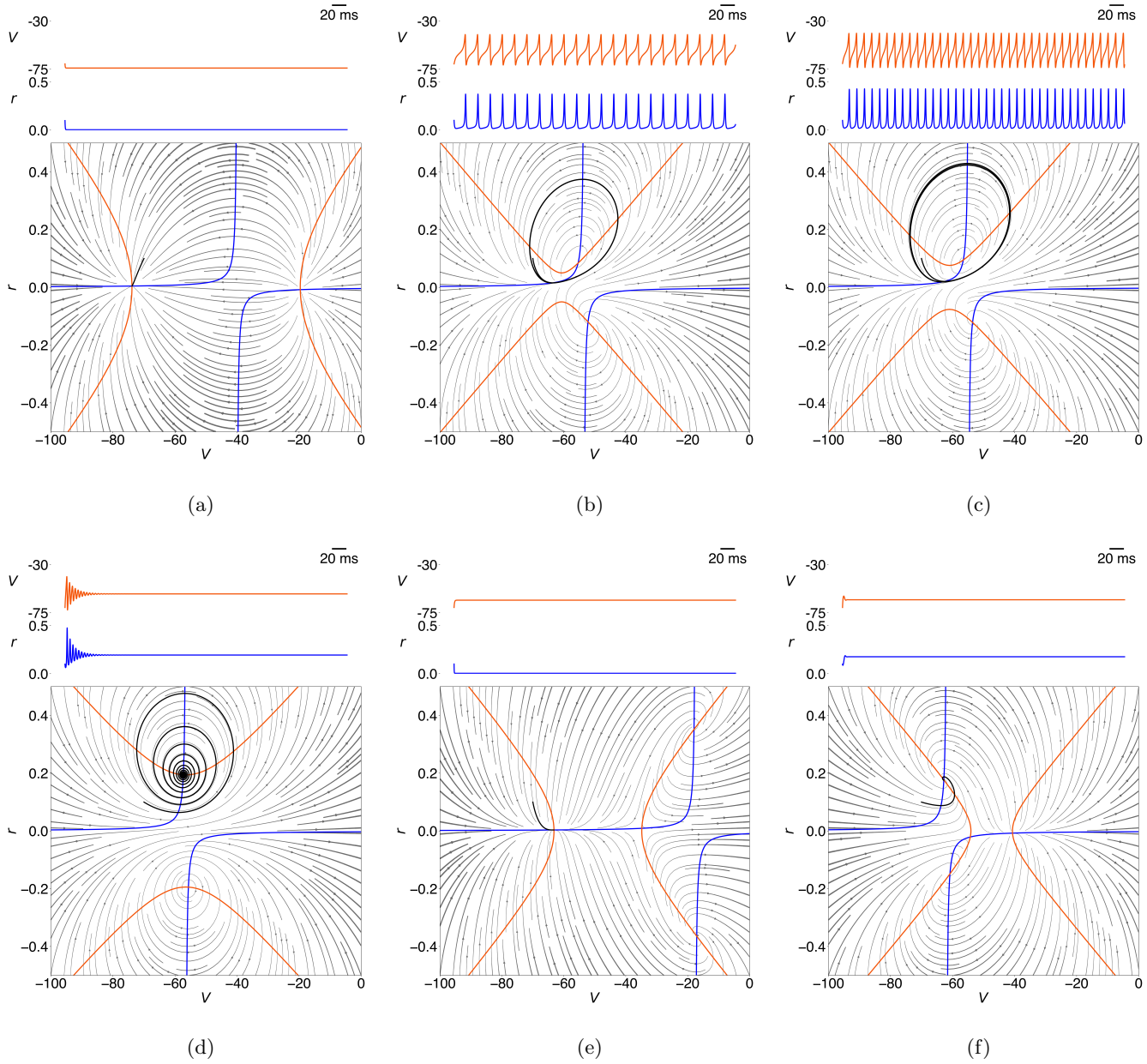

Figure 2: Phase-planes of the $r - V$ subsystem. (a) fixed point for u=21, S_a=0.04, $[D_p]$=0.8. (b) limit-cycle obtained considering u=7.9, S_a=0.051, $[D_p] = 7.7e^{-4}$, (c) limit-cycle obtain for u=10, S_a=0.06, $[D_p] = 1e^{-5}$, (d) Dumped oscillations u=100, S_a=0.15, $[D_p]$=0.5. (e) bistability with upper stable focus and a lower for r negative with u=70, S_a=0.3, $[D_p]$=0.1. (f) bistable regime with a lower fixed point and upper stable focus with u=70, S_a=0.004, $[D_p]$=25, All temporal simulations were conducted considering initial conditions (r_0, V_0) = (0.1, -70.0), values close to resting state.

To understand the structure underlying these emergent behaviors, we did a bifurcation analysis,

considering the slow variable u and the two variables associated with external inputs: S_a which will be modulated by c_{exc} corresponding to excitatory input and $[D_p]$ that will be modulated by c_{dopa} the dopaminergic input.

The results are presented in Figure 3. Variable influence on the fast sub-system $r - V$ was analyzed varying jointly with the input from two other variables considered constant. The first investigation was on the $D_p - u$ influence on the behavior. We can identify the oscillatory regime where two green surfaces, corresponding to unstable focuses, appear in Figure 3a, which correspond for D_p between 0 to 0.75 and u between 0 and 35, (regions corresponding to the tight south-west – north-east hatching in the projection in Figure 3d). This specific regime can be observed in the space of $S_a - D_p$ (Figure 3b) for values of S_a starting from 0.8 and D_p up to 0.8 (Figure 3e). The 4 fixed points regime is also shown with the existence of the saddle node, in purple for the 3-dimensional Figures (3a, 3b, 3c) and with vertical hatches for the projection Figures (3d, 3e, 3f). The slow variable u enables the bursting activities as shown in previous works [6, 19].

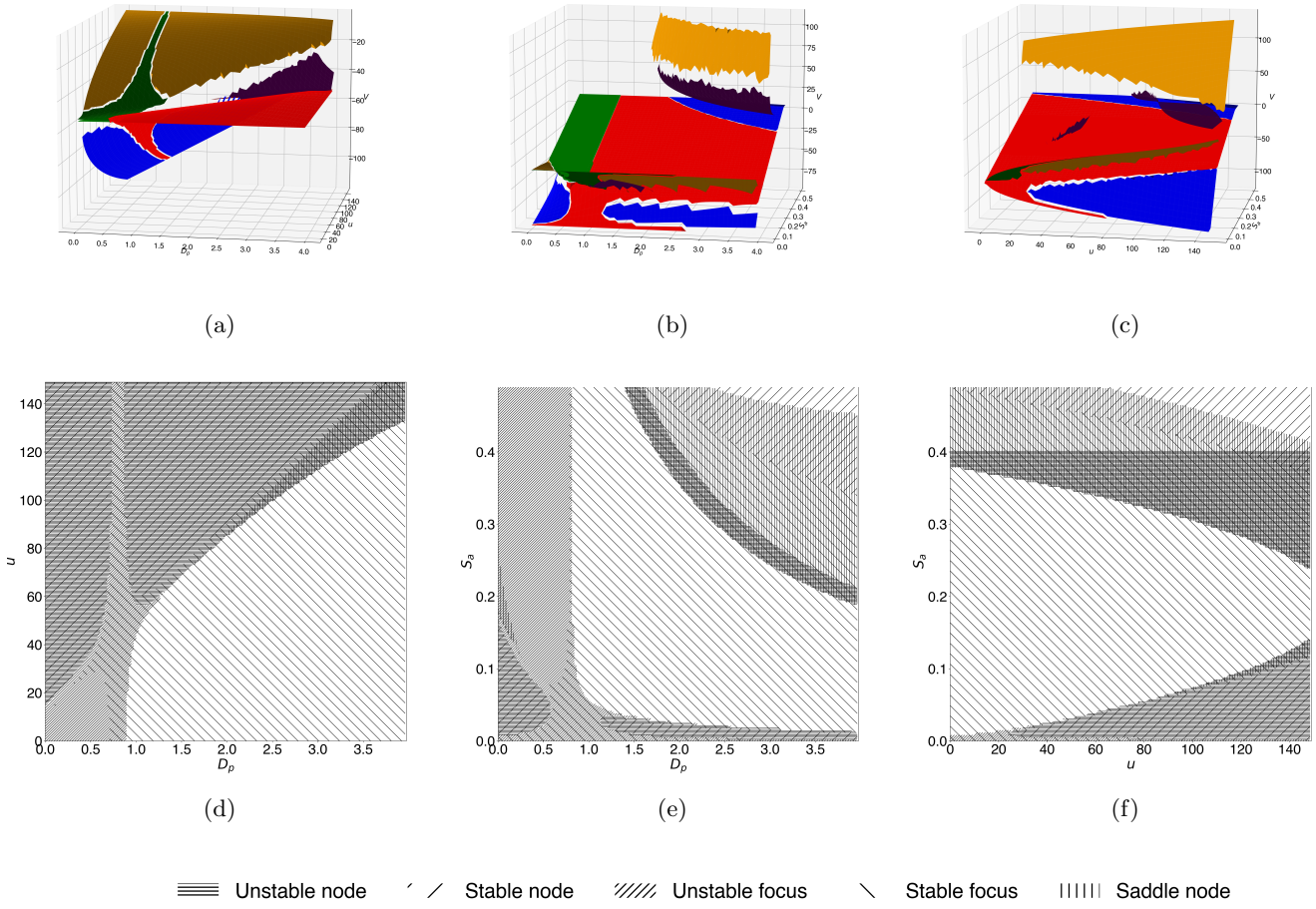

Figure 3: Structure of the fixed points of the $r - V$ sub system. (a) 3D structure of the V coordinates depending on the values of D_p and u variables, with S_a fixed at 0.06. (b) 3D structure of the V coordinates depending on the values of D_p and S_a variables, with u fixed at 120. (c) 3D structure of the V coordinates depending on the values of u and S_a variables, with $[D_p]$ fixed at 2. (a, b, c) Unstable nodes are in orange, stable nodes in blue, unstable focus in green, stable focus in red and saddle-node in purple. (d, e, f) Projections of the structure are presented respectively in panels a, b, c. In these last three panels, we can identify regions of coexistence of fixed-point.

Considering a fixed $u = 10$, taking D_p as the bifurcation parameter, we can observe the oscillatory regime mentioned before for values of D_p going from 0 to around 0.75 (Figures 4a, 4b). These oscillations are limit-cycles, with amplitude represented by the grey line in Figures 4a, 4b. Another interesting slice is with u fixed to 120 on which we can observe the alternance of unstable node and unstable focus and, with greater values of D_p, the appearance of the 4-equilibrium points (Figures 4c, 4d).

One important observation is the existence of stable attractors in the negative range of the variable r which corresponds to the firing rate. However, these stable attractors are unrealistic. When using the model for simulation purposes, users should ensure that the trajectory remains in the basin of attraction of r positive values.

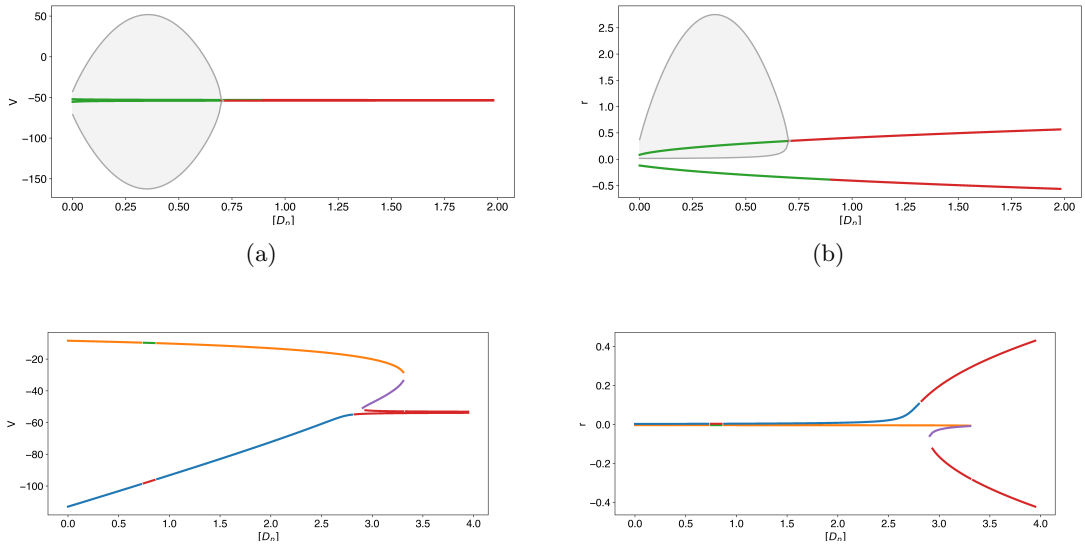

Figure 4: bifurcation diagrams: (a) and (b) respectively for V and r, along D_p values (with fixed $u = 10$ and $S_a = 0.06$), the gray area corresponds to the amplitude of the limit-cycle existing around unstable focuses (in green), fixed-point in red are stable focuses. (c) and (d) respectively for V and r, along D_p values (with fixed $u = 120$ and $S_a = 0.06$) Unstable nodes are in orange, stable nodes in blue, unstable focus in green, stable focus in red, and saddle-node in purple

3.2 Full system dynamics

After having described the possible dynamics of the fast $r - V$ subsystem, we can now present the dynamical repertoire of the complete system of equations. The number of dimensions does not enable the analytical study of the dynamical structure. In this section, we present the results of numerical simulations (10s longs) of the model for different values of external inputs c_{exc} and c_{dopa}. After eliminating the transient period of 2 seconds, allowing the system to stabilize and reach a steady-state, we not only focus on the mean firing rate but also on the standard deviation to identify zones where the dynamics undergo significant changes. These metrics are presented in Figure 5, where various qualitative behaviors are illustrated, as also depicted in Figure 6. Specifically, fixing the excitation value (for instance, $c_{exc} \sim 1.4e-1$), it is evident that as c_{dopa} increases, both the

average firing rate and the standard deviation also increase. This is demonstrated in panels (6d) and (6e), where there is a noticeable increase in the amplitude of oscillations; this means that the system is characterized by an oscillatory behavior well synchronized. With a further increase in c_{dopa} approaching the separation line visible in the referenced Figure 6, the system transitions from an oscillatory to a bistable regime (6a-c), and the amplitude of each oscillation grows, becoming less synchronized. Beyond this boundary, the dynamics settle into a stable fixed point, similar to the scenario at lower c_{dopa}, albeit at a different and higher value for each variable of interest (6f).

Thus, we demonstrate the dopaminergic effect on a single node; indeed, changes in dopamine parameters affect qualitatively the dynamics of the system.

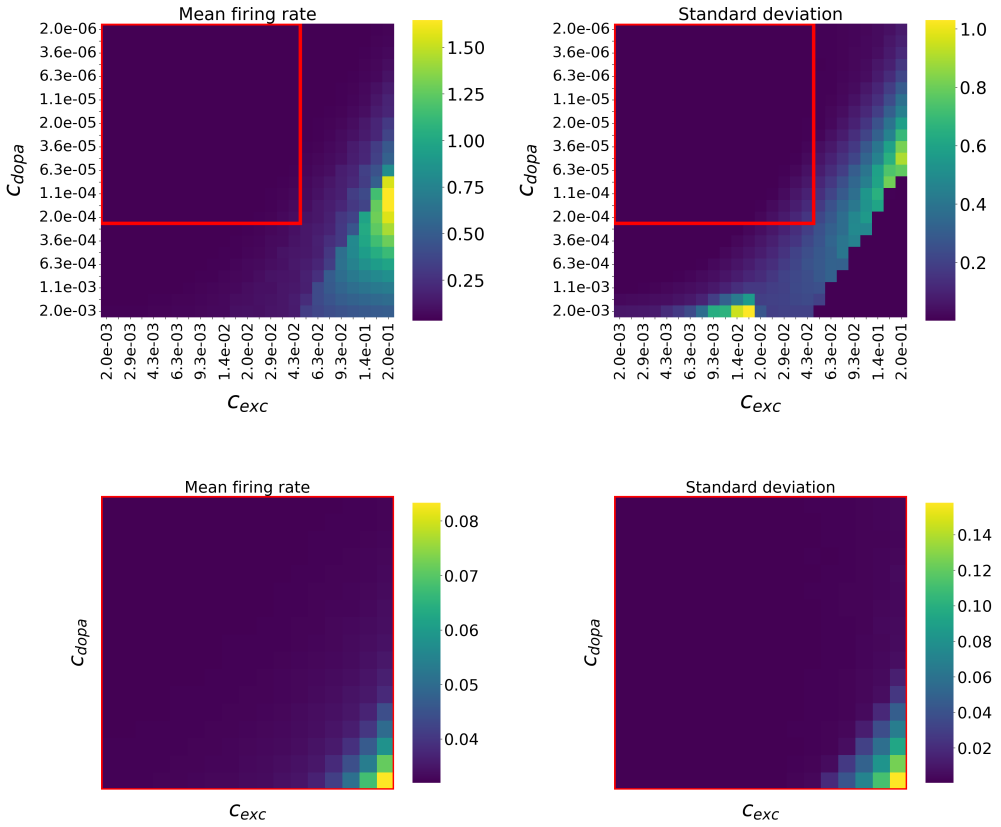

Figure 5: Effects of excitatory and dopaminergic inputs on a single neural node, with the mean firing rate shown on the left and its standard deviation on the right. In the pictures, the colour gradient transitions from purple to yellow, marking the shift from the lowest to the highest values observed. The highest mean firing rates occur at elevated levels of both excitatory and dopaminergic inputs. A red square highlights a specific area of interest, and the effects within this region —both in terms of firing rate and standard deviation— are detailed in the bottom row of the figure.

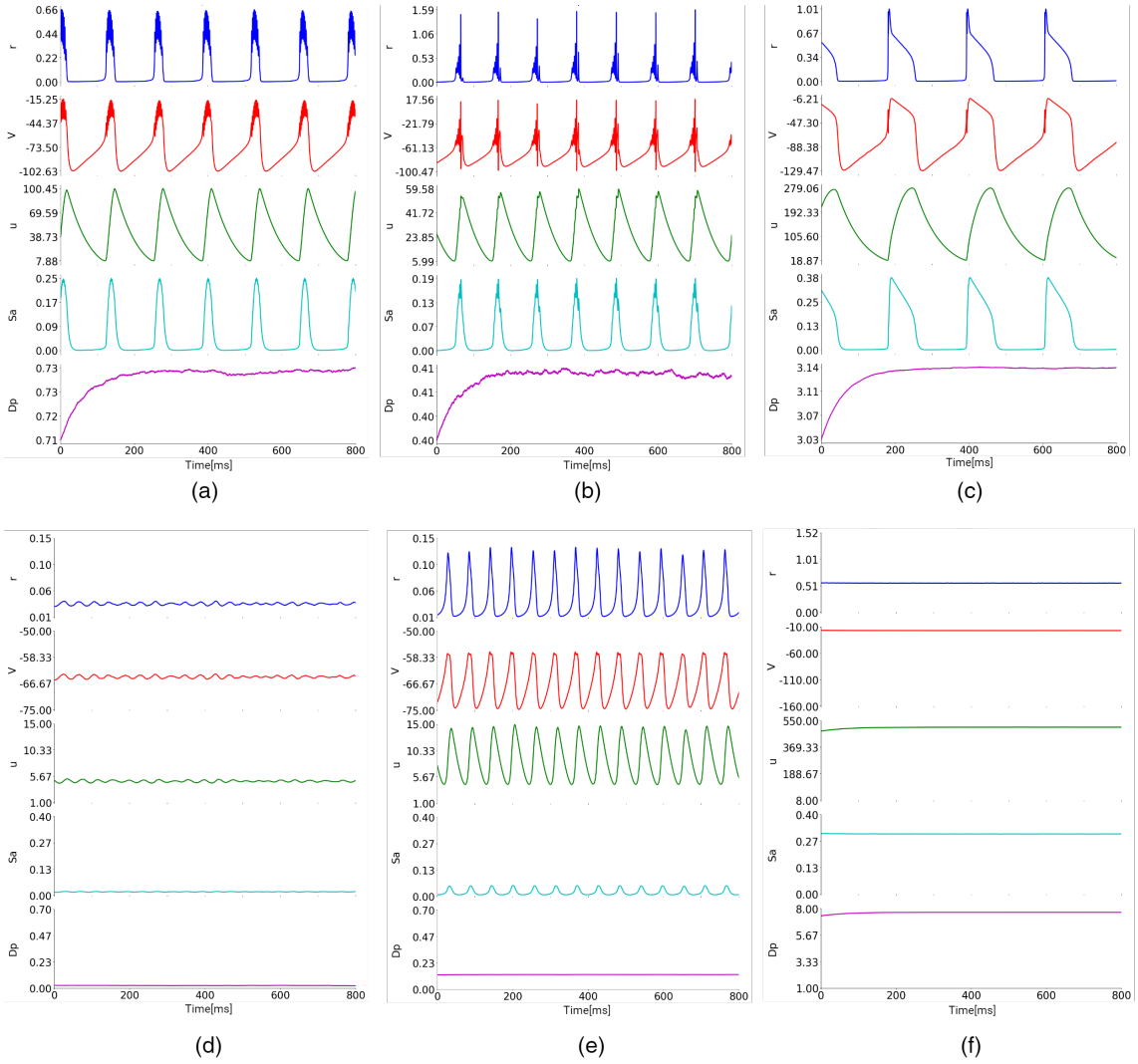

Figure 6: Time series of the system variables to understand the qualitative change in the dynamics of the system as the parameters c_{exc} and c_{dopa} change, using a noise parameter equal to 1e-4. Each panel of the figure represents the dynamics for some fixed values of the two parameters. Specifically, fixing the excitation value at $\sim 1.4e1$ (in all panels) and increasing c_{dopa}, the system goes from an oscillatory regime where the amplitude of each oscillation grows with values for (d) $c_{dopa} \sim 2e-6$ and (e) $c_{exc} \sim 1.4e-1$) to a bistable regime (a) $c_{dopa} \sim 6.3e-5$, (b) $c_{dopa} \sim 3.6e-5$, and (c) $c_{dopa} \sim 2.7e-4$. For the lowest to highest c_{dopa} value we can notice how the dynamics of the system are focused around a fixed point, but it becomes higher for high c_{dopa} values (f) $c_{dopa} > 6.3e-4$.

3.3 Basal Ganglia network

This model is employed to construct a representation of the basal ganglia network. The basal ganglia network constitutes a sophisticated arrangement of subcortical nuclei critically involved

in motor control, reward processing, and cognitive functions. Its constituent nuclei include the striatum (comprising the caudate nucleus and putamen), globus pallidus (segmented into internal and external segments, GPi and GPe), substantia nigra (consisting of the pars compacta and pars reticulata), and the subthalamic nucleus. The striatum, as the principal input nucleus, receives projections from diverse cortical regions, integrating and processing this information. Subsequently, it influences the GPi and GPe, which serve as the primary output nuclei, orchestrating motor responses through intricate inhibitory and excitatory pathways.

The interplay of inhibitory and excitatory signals within the basal ganglia network is highly nuanced. The GPe and GPi predominantly exert inhibitory control, transmitting signals to the thalamus and brainstem motor centers, thereby regulating motor output. Conversely, the subthalamic nucleus provides excitatory input to the GPi, contributing to the finely tuned balance of the network. This balance is pivotal for the precise modulation of motor functions. Dysregulation in these inhibitory-excitatory dynamics is implicated in neurodegenerative disorders such as PD.

In this small example, we show how the network effect enables the emergence of different behaviors. In Figure 7, we show that changing the weights of the dopamine projection from Substentia Negra Pars Compacta (SNc) to Dorsal Striatum affects the dynamics of the basal ganglia network. In this example, we observed changes in the frequency content and the emergence of a peak in the range of the spectrum. Such peaks in frequency are observed in pathological conditions such as in PD [30].

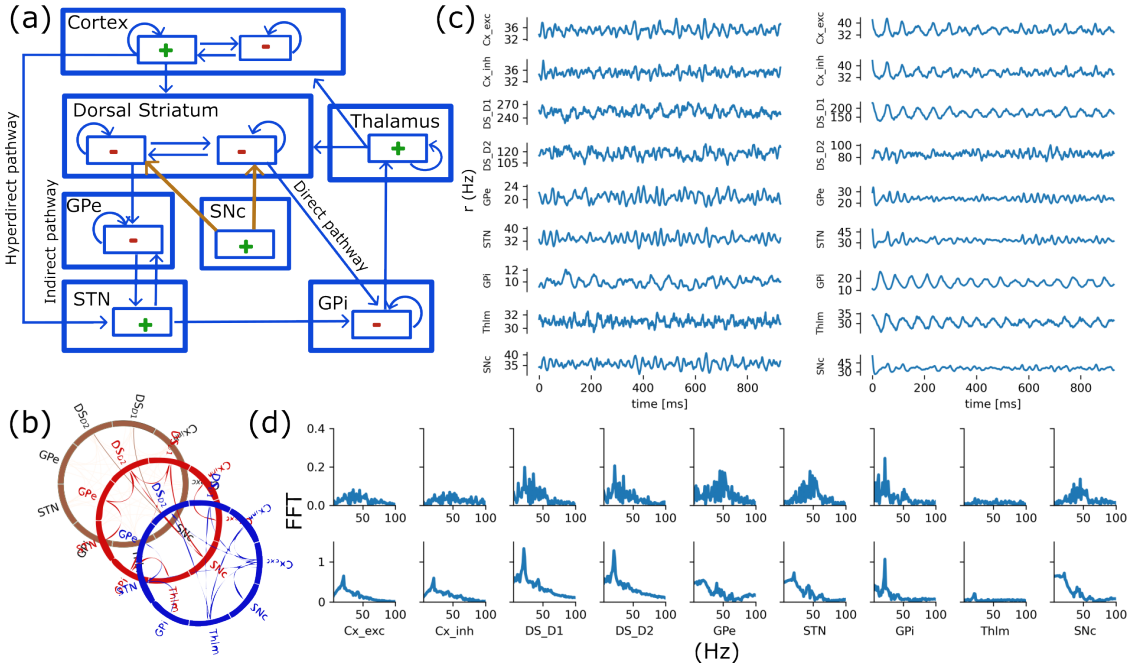

Figure 7: Basal Ganglia Network simulation: (a) Simplified basal ganglia network schematic adapted from [8] (b) The network is built with 3 layers of connectivity between nodes: excitatory, inhibitory, dopaminergic, (c) Firing rate of each node for 10-second simulations: on the left "Healthy" resting state simulation, on the right impaired dopamine projection (i.e. weights decreased by half) from substantia negra pars compacta to dorsal striatum D1 population. (d) On the first row is the fast-Fourier transform of the "Healthy" resting state condition, where no specific peaks appear. On the second row, corresponding to the impaired condition, peaks appear and notably in the β range of frequency.

4 Discussion

We proposed a modeling framework to capture the effects of neuromodulator dynamics on the neuronal electrophysiological activity at a neural mass level. We gave results on a reduced version, specific for dopamine dynamics. We show the dynamical repertoire associated with the level of dopamine and we validate the novel implementation with an example model of the basal ganglia network.

Such an approach enables us to obtain the dynamical repertoire with a reduced number of variables that can still be interpreted or associated with meaningful biophysical units. Indeed, while the proposed model is phenomenological in nature, it serves to capture the evolution of physical variables that can be directly related to observables, such as firing rates, mean membrane potentials, and synaptic currents.

One novelty of the framework presented here is the expression of the action of dopamine as a scaling of the synaptic conductance at the mesoscopic neural mass model level, this formulation can in fact be seen as a natural extension of the seminal works of Humphries [17] and Durstewitz [11, 12] in which dopaminergic action was modeled as such on the microscopic level of individual spiking neurons. This latter approach was also employed in [28] to capture the effects of dopamine depletion in a spiking neural network model of the basal ganglia. As such, our proposed form for dopamine action on the neural mass model builds on previous work of validated biophysical models of spiking neurons to provide a computationally efficient framework that extends the modeling of dopaminergic neuromodulatory action from the level of populations of spiking neurons to that of the whole brain network level.

This modeling framework also enables the introduction of other receptors, such as NMDA [46]. The framework is modular in function of the application. It makes it a good candidate to be used in personalized brain models, in the context of virtual brain twins.

Virtual brain twins represent a novel concept, where only specific features of interest to a neurological condition are captured by the model to be related to corresponding clinical data [50]. This method can go a step further and tailor the model to the patient's brain. This approach involves simulating subject-specific brain structures to aid in the diagnosis and treatment of brain disorders or to gain deeper insights into the healthy brain. By tailoring the modeling to individual subjects, researchers can better understand the intricacies of brain function and pathology. In Wang et al. [50], the standard model was presented in a generic format, including local dynamics with both global and local connectivity. With this work, we present one of the first detailed and concrete models that could serve as a standard model for brain dynamics on a mesoscopic level. In ongoing works, we are utilizing this model as the foundation for virtual brain twins, particularly in the context of PD and psychiatric disorders.

5 Acknowledgment

The preparation of this article was funded through the EU's Horizon Europe Programme SGA 101147319 (EBRAINS 2.0), and SGA 101137289 (virtual brain twin). We acknowledge the support of the Government of Canada's New Frontiers in Research Fund (NFRF).

List of variables and parameters

The model is unitless by definition, however, some of the variables and parameters can be "associated phenomenologically" with measurable biophysical units. We detail the parameter values and the units that could be conceptually associated with in table 5.

	Variables	**Symbol**	**Associated unit**
Neuromodulation	Firing rate	r	kHz
neural mass	Mean membrane potential	V	mV
	Adaptation	u	nA
	AMPA synapses activation	S_a	-
	GABA synapses activation	S_g	-
	Extracellular dopamine concentration	$[D_p]_e$	mM
	D1 dopamine receptor modulation	M_{D1}	-

Parameters	Symbol	Value	Associated unit
aQIF parameter	a	0,04	-
aQIF parameter	b	5	-
aQIF parameter	c	140	-
aQIF parameter	α	0,013	-
aQIF parameter	β	0,4	-
Mean additive current	η	18	nA
Maximal conductance of AMPA	g_a	12	nS
Maximal conductance of GABA	g_g	12	nS
Additive current half-width distribution	Δ	1	-
Linearization factor of dopaminergic receptors	A_{D_p}	1	nS/mM
Basal level in absence of neuromodulation	B	0,2	nS
Reversal potential of AMPA synapses	E_a	0	mV
Reversal potential of GABA synapses	E_g	-80	mV
External current	I_{ext}	0	nA
Adaptation step	u_d	12	nA
Time constant of AMPA synapses	τ_{S_a}	5	ms
Time constant of GABA synapses	τ_{S_g}	5	ms
Time constant of dopamine concentration evolution	τ_{D_p}	500	ms
Time constant of dopamine receptor modulation	τ_m	500	ms
Strength of AMPA synapses	S_{ja}	0,8	nS
Strength of GABA synapses	S_{jg}	1,2	nS
Excitatory coupling	c_{exc}	-	kHz
Inhitatory coupling	c_{inh}	-	kHz
Dopamine coupling	c_{dopa}	-	mM
Maximum dopamine reuptake rate	V_{max}	1300	mM/s
Michaelis constant	K_m	150	mM
Dopamine coupling factor	k	100 000	-
Receptor density	R_d	1	-
Receptor sensitivity to dopamine	S_p	1	-
Noise standard deviation	σ	1e-3	-

References

[1] Katrin Amunts, Markus Axer, Swati Banerjee, Lise Bitsch, Jan G Bjaalie, Philipp Brauner, Andrea Brovelli, Navona Calarco, Marcel Carrere, Svenja Caspers, et al. The coming decade

of digital brain research: A vision for neuroscience at the intersection of technology and computing. *Imaging Neuroscience*, 2:1–35, 2024.

[2] R. Balestrino and A. H.V. Schapira. Parkinson disease. *European Journal of Neurology*, 27(1):27–42, 2020.

[3] Anne S Berry, Vyoma D Shah, Suzanne L Baker, Jacob W Vogel, James P O'Neil, Mustafa Janabi, Henry D Schwimmer, Shawn M Marks, and William J Jagust. Aging affects dopaminergic neural mechanisms of cognitive flexibility. *Journal of Neuroscience*, 36(50):12559–12569, 2016.

[4] Rasmus M. Birn, Alexander K. Converse, Abigail Z. Rajala, Andrew L. Alexander, Walter F. Block, Alan B. McMillan, Bradley T. Christian, Caitlynn N. Filla, Dhanabalan Murali, Samuel A. Hurley, Rick L. Jenison, and Luis C. Populin. Changes in endogenous dopamine induced by methylphenidate predict functional connectivity in nonhuman primates. *The Journal of Neuroscience*, 39(8):1436–1444, December 2018.

[5] Ethan S. Bromberg-Martin, Masayuki Matsumoto, and Okihide Hikosaka. Dopamine in motivational control: Rewarding, aversive, and alerting. *Neuron*, 68(5):815–834, December 2010.

[6] Liang Chen and Sue Ann Campbell. Exact mean-field models for spiking neural networks with adaptation. *Journal of Computational Neuroscience*, jul 2022.

[7] Martin J Dahl, Shelby L Bachman, Shubir Dutt, Sandra Düzel, Nils C Bodammer, Ulman Lindenberger, Simone Kühn, Markus Werkle-Bergner, and Mara Mather. The integrity of dopaminergic and noradrenergic brain regions is associated with different aspects of late-life memory performance. *Nature Aging*, 3(9):1128–1143, 2023.

[8] Mahlon R. DeLong. Primate models of movement disorders of basal ganglia origin. *Trends in Neurosciences*, 13(7):281–285, July 1990.

[9] Damien Depannemaecker, Aitakin Ezzati, Huifang E. Wang, Viktor Jirsa, and Christophe Bernard. From phenomenological to biophysical models of seizures. *Neurobiology of Disease*, 182:106131, June 2023.

[10] Damien Depannemaecker, Anton Ivanov, Davide Lillo, Len Spek, Christophe Bernard, and Viktor Jirsa. A unified physiological framework of transitions between seizures, sustained ictal activity and depolarization block at the single neuron level. *Journal of Computational Neuroscience*, 50(1):33–49, January 2022.

[11] Daniel Durstewitz. Dopaminergic modulation of prefrontal cortex network dynamics. In *Monoaminergic Modulation of Cortical Excitability*, pages 217–234. Springer, 2007.

[12] Daniel Durstewitz, Marian Kelc, and Onur Güntürkün. A neurocomputational theory of the dopaminergic modulation of working memory functions. *Journal of Neuroscience*, 19(7):2807–2822, 1999.

[13] Egidio D'Angelo and Viktor Jirsa. The quest for multiscale brain modeling. *Trends in neurosciences*, 2022.

[14] Martin Ebert, Christian Hauptmann, and Peter A. Tass. Coordinated reset stimulation in a large-scale model of the STN-GPE circuit. *Frontiers in Computational Neuroscience*, 8(NOV):1–20, 2014.

[15] Carole Guedj, Elisabetta Monfardini, Amélie J Reynaud, Alessandro Farnè, Martine Meunier, and Fadila Hadj-Bouziane. Boosting norepinephrine transmission triggers flexible reconfiguration of brain networks at rest. *Cerebral Cortex*, September 2016.

[16] Oliver D. Howes and Ekaterina Shatalina. Integrating the neurodevelopmental and dopamine hypotheses of schizophrenia and the role of cortical excitation-inhibition balance. 92(6):501–513.

[17] Mark D Humphries, Nathan Lepora, Ric Wood, and Kevin Gurney. Capturing dopaminergic modulation and bimodal membrane behaviour of striatal medium spiny neurons in accurate, reduced models. *Frontiers in computational neuroscience*, 3:849, 2009.

[18] E.M. Izhikevich. Simple model of spiking neurons. *IEEE Transactions on Neural Networks*, 14(6):1569–1572, 2003.

[19] Eugene M. Izhikevich. *Dynamical Systems in Neuroscience: The Geometry of Excitability and Bursting*. The MIT Press, 2006.

[20] Renaud Jardri and Sophie Denève. Circular inferences in schizophrenia. *Brain*, 136:3227–3241, 11 2013.

[21] Kenneth A. Johnson and Roger S. Goody. The original michaelis constant: Translation of the 1913 michaelis–menten paper. *Biochemistry*, 50(39):8264–8269, September 2011.

[22] Kyesam Jung, Esther Florin, Kaustubh R. Patil, Julian Caspers, Christian Rubbert, Simon B. Eickhoff, and Oleksandr V. Popovych. Whole-brain dynamical modelling for classification of Parkinson's disease. *Brain Communications*, 5(1):1–19, 2023.

[23] JP Kesby, DW Eyles, JJ McGrath, and JG Scott. Dopamine, psychosis and schizophrenia: the widening gap between basic and clinical neuroscience. *Translational Psychiatry*, 8(1), January 2018.

[24] Marianne O. Klein, Daniella S. Battagello, Ariel R. Cardoso, David N. Hauser, Jackson C. Bittencourt, and Ricardo G. Correa. Dopamine: Functions, signaling, and association with neurological diseases. *Cellular and Molecular Neurobiology*, 39(1):31–59, November 2018.

[25] Morten L. Kringelbach, Josephine Cruzat, Joana Cabral, Gitte Moos Knudsen, Robin Carhart-Harris, Peter C. Whybrow, Nikos K. Logothetis, and Gustavo Deco. Dynamic coupling of whole-brain neuronal and neurotransmitter systems. *Proceedings of the National Academy of Sciences*, 117(17):9566–9576, April 2020.

[26] Mario Lavanga, Johanna Stumme, Bahar Hazal Yalcinkaya, Jan Fousek, Christiane Jockwitz, Hiba Sheheitli, Nora Bittner, Meysam Hashemi, Spase Petkoski, Svenja Caspers, et al. The virtual aging brain: Causal inference supports interhemispheric dedifferentiation in healthy aging. *NeuroImage*, 283:120403, 2023.

[27] Antonio F Leuchter, Stephanie McKinney, Viraj Desai, and John T McCracken. Serotonin dysfunction, aggressive behavior, and mental illness: Exploring the link using a dimensional approach. *Current Neuropharmacology*, 14(7).

[28] Mikael Lindahl and Jeanette Hellgren Kotaleski. Untangling basal ganglia network dynamics and function: Role of dopamine depletion and inhibition investigated in a spiking network model. *eneuro*, 3(6), 2016.

[29] Simon Little, Martijn Beudel, Ludvic Zrinzo, Thomas Foltynie, Patricia Limousin, Marwan Hariz, Spencer Neal, Binith Cheeran, Hayriye Cagnan, James Gratwicke, et al. Bilateral adaptive deep brain stimulation is effective in parkinson's disease. *Journal of Neurology, Neurosurgery & Psychiatry*, 87(7):717–721, 2016.

[30] Simon Little and Peter Brown. The functional role of beta oscillations in parkinson's disease. *Parkinsonism amp; Related Disorders*, 20:S44–S48, January 2014.

[31] Robert A. McCutcheon, Anissa Abi-Dargham, and Oliver D. Howes. Schizophrenia, dopamine and the striatum: From biology to symptoms. 42(3):205–220.

[32] M.L. Michaelis, L. Menten. Die kinetik der invertinwirkung. *Biochem Z*, 1913.

[33] CRISTINA MISSALE, S. RUSSEL NASH, SUSAN W. ROBINSON, MOHAMED JABER, and MARC G. CARON. Dopamine receptors: From structure to function. *Physiological Reviews*, 78(1):189–225, January 1998.

[34] Joanna Moncrieff, Ruth E. Cooper, Tom Stockmann, Simone Amendola, Michael P. Hengartner, and Mark A. Horowitz. The serotonin theory of depression: a systematic umbrella review of the evidence. *Molecular Psychiatry*, 7 2022.

[35] Ernest Montbrió, Diego Pazó, and Alex Roxin. Macroscopic description for networks of spiking neurons. *Physical Review X*, 5(2), jun 2015.

[36] David J Nutt, DJ Nutt, Robin L Carhart-Harris, DJ Nutt, Michael J Forsythe, and DJ Nutt. The serotonin theory of depression: a systematic umbrella review of the evidence. *Nature Reviews Neuroscience*, 23(2):119–133, 2022.

[37] Institute of Health Metrics and Evaluation. Global health data exchange (ghdx). Technical report, (https://vizhub.healthdata.org/gbd-results/), May 2022.

[38] Carlos A. Paladini, Siobhan Robinson, Hitoshi Morikawa, John T. Williams, and Richard D. Palmiter. Dopamine controls the firing pattern of dopamine neurons via a network feedback mechanism. *Proceedings of the National Academy of Sciences*, 100(5):2866–2871, February 2003.

[39] Tamara Pringsheim, Nathalie Jette, Alexandra Frolkis, and Thomas D.L. Steeves. The prevalence of Parkinson's disease: A systematic review and meta-analysis. *Movement Disorders*, 29(13):1583–1590, 2014.

[40] Joshua L. Roffman, Alexandra S. Tanner, Hamdi Eryilmaz, Anais Rodriguez-Thompson, Noah J. Silverstein, New Fei Ho, Adam Z. Nitenson, Daniel B. Chonde, Douglas N. Greve, Anissa Abi-Dargham, Randy L. Buckner, Dara S. Manoach, Bruce R. Rosen, Jacob M. Hooker, and Ciprian Catana. Dopamine d 1 signaling organizes network dynamics underlying working memory. *Science Advances*, 2(6), June 2016.

[41] Maria Luisa Saggio, Andreas Spiegler, Christophe Bernard, and Viktor K. Jirsa. Fast–slow bursters in the unfolding of a high codimension singularity and the ultra-slow transitions of classes. *The Journal of Mathematical Neuroscience*, 7(1), July 2017.

[42] T. Sakaguchi and G.A. Bray. Effect of norepinephrine, serotonin and tryptophan on the firing rate of sympathetic nerves. *Brain Research*, 492(1–2):271–280, July 1989.

[43] Paula Sanz-Leon, Stuart A Knock, Andreas Spiegler, and Viktor K Jirsa. Mathematical framework for large-scale brain network modeling in the virtual brain. *Neuroimage*, 111:385–430, 2015.

[44] Wolfram Schultz. Multiple dopamine functions at different time courses. *Annu. Rev. Neurosci.*, 30:259–288, 2007.

[45] Golia Shafiei, Yashar Zeighami, Crystal A Clark, Jennifer T Coull, Atsuko Nagano-Saito, Marco Leyton, Alain Dagher, and Bratislav Mišić. Dopamine signaling modulates the stability and integration of intrinsic brain networks. *Cerebral Cortex*, 29(1):397–409, October 2018.

[46] Hiba Sheheitli and Viktor Jirsa. Incorporating slow nmda-type receptors with nonlinear voltage-dependent magnesium block in a next generation neural mass model: derivation and dynamics. *Journal of Computational Neuroscience*, to appear.

[47] Xiu Sun, Yun Zhao, and Marina E. Wolf. Dopamine receptor stimulation modulates ampa receptor synaptic insertion in prefrontal cortex neurons. *The Journal of Neuroscience*, 25(32):7342–7351, August 2005.

[48] Peter A. Tass. A model of desynchronizing deep brain stimulation with a demand-controlled coordinated reset of neural subpopulations. *Biological Cybernetics*, 89(2):81–88, 2003.

[49] Janita Turchi, Catie Chang, Frank Q. Ye, Brian E. Russ, David K. Yu, Carlos R. Cortes, Ilya E. Monosov, Jeff H. Duyn, and David A. Leopold. The basal forebrain regulates global resting-state fmri fluctuations. *Neuron*, 97(4):940–952.e4, February 2018.

[50] Huifang E Wang, Paul Triebkorn, Martin Breyton, Borana Dollomaja, Jean-Didier Lemarechal, Spase Petkoski, Pierpaolo Sorrentino, Damien Depannemaecker, Meysam Hashemi, and Viktor K Jirsa. Virtual brain twins: from basic neuroscience to clinical use. *National Science Review*, 11, 4 2024.

[51] Evan Weiss, Michael Kann, and Qi Wang. Neuromodulation of neural oscillations in health and disease. *Biology*, 12(3):371, February 2023.

[52] Zixiao Yin, Guanyu Zhu, Baotian Zhao, Yutong Bai, Yin Jiang, Wolf Julian Neumann, Andrea A. Kühn, and Jianguo Zhang. Local field potentials in Parkinson's disease: A frequency-based review. *Neurobiology of Disease*, 155:105372, 2021.

[53] Ying Yu, Xiaomin Wang, Qishao Wang, and Qingyun Wang. A review of computational modeling and deep brain stimulation: applications to Parkinson's disease. *Applied Mathematics and Mechanics (English Edition)*, 41(12):1747–1768, 2020.